Preparation method and luminescent properties of $Ca_{7-x}Sr_xSi_2P_2O_{16}:Eu^{3+}$ red-emitting phosphors

JUNFENG LI, WENQIANG CAO, YUQING LIU, YANG GAO, WENTAO ZHANG, PEICONG ZHANG
College of Materials, Chemistry & Chemical Engineering, Chengdu University of Technology, Chengdu 610059, Sichuan, P.R.China

The $Ca_{7-x}Sr_xSi_2P_2O_{16}:Eu^{3+}$ red phosphors were prepared by the sol-gel process and the phase and photoluminescence properties of the prepared phosphors were respectively characterized by the X-ray powder diffraction (XRD) analysis and photoluminescence analysis. The characterization results indicated that the single $Ca_7Si_2P_2O_{16}$ with hexagonal crystal structure was successfully synthesized at 1500 °C for 5 h. Under ultraviolet excitation, $Ca_{7-x}Sr_xSi_2P_2O_{16}:Eu^{3+}$ showed several absorption peaks ranging from 210 nm to 550 nm and a broad red emission band with the peak at 617 nm. In addition, we also explored the influences of different concentrations of Eu^{3+} ions and Sr^{2+} ions on the emission intensity and the phases. The results demonstrated that the phosphor was a better red light-emitting material.

(Received February 26, 2016; accepted February 10, 2017)

Keywords: Luminescence; Phosphor, $Ca_{7-x}Sr_xSi_2P_2O_{16}$; Sol-gel, White light emitting diode

1. Introduction

As a solid-green environmental light source, white light emitting diodes (WLEDs) have been considered as the most valuable new light source in the 21st century [1-3]. Though WLEDs have been widely applied in many fields such as light emitting display, laser device, and biomedicine [4-5], red luminescence used for LED, especially the red phosphor with high efficiency and stability, are seldom reported, thus resulting in poor color rendering index and greatly restricting the application of WLEDs [6-8].

Compared with traditional sulfide and aluminate phosphors [9-10], the silicate phosphors possess the advantages of high light conversion efficiency, high crystallinity, wide excitation spectrum, and high chemical and thermal stability, and the raw materials for preparing silicate phosphors are cheap [11-12]. However, the performance of silicate red powder is not excellent enough for WLEDs. In recent years, the luminescent intensity enhancement of phosphors with partial cation substitution has been reported. Yongqing Zhai synthesized $SrMgSi_2O_6:Eu^{3+}$ red silicate phosphor and increased the emission intensity remarkably by partially substituting Si^{4+} with Ti^{4+}[13]. Hongli Liu synthesized $(Ba_{1-X}Sr_X)_2SiO_4:Eu^{2+}$ via high-temperature solid state method and found that the phosphors could exhibit strong red light at 598 nm under the excitation wavelength at 395 nm and that the emission turned out to be a red shift with the increase of x [14]. In addition, anionic modification was also adopted to improve the luminescent intensity of phosphors. For example, halogen elements were used to prepare orange phosphors by replacing partial anionic silicate matrix to obtain $Ca_3SiO_4Cl_2:Eu^{2+}$ [15]. Based on the silicate system, phosphate was used to replace partial silicate in the silicate matrix [16-20]. Jiuhu Gan studied the $Sr_5(PO_4)_2(SiO_4):Eu^{2+}$ for green-emitting phosphor [21]. Donglei Wei and Yurong Shi explored luminescence applications of $Ca_7Si_2P_2O_{16}:xEu^{2+}$ prepared through the solid-state reaction method [22-23].

Previous studies on silicon host phosphate were focused on single cation doping modification or anionic substitution modification as well as the luminescent properties of Eu^{2+}-doped phosphate phosphor with anionic substitution modification. On the basis of the studies on Eu^{3+} doped silicon phosphate phosphor, the study aims to study cationic and anionic co-doped silicon phosphate phosphors and further explore Eu^{3+} doped $Ca_7Si_2P_2O_{16}$ phosphors by replacing Ca^{2+} with Sr^{2+}. The effect of Sr^{2+} substitution on the structure and luminescent intensity was discussed in detail. Based on the typical fluorescent powder of silicon phosphate system, we experimentally prepared Eu^{3+}-excited silicon phosphor by co-doping of cation and anion.

2. Experimental

The major raw materials included $Ca(NO_3)_2{\cdot}4H_2O$, $Sr(NO_3)_2$, $NH_4H_2PO_4$, tetraethyl silicate ($Si(OC_2H_5)_4$, TEOS), Eu_2O_3, and citric acid ($C_6H_8O_7{\cdot}H_2O$). Eu_2O_3 was

dissolved in the HNO_3 and then the solution was mixed with $Ca(NO_3)_2{\cdot}4H_2O$, $NH_4H_2PO_4$, and citric acid in the deionized water. After that, tetraethyl silicate (TEOS) was added into the mixed solution and then absolute ethanol was dropwise added and stirred until the gels were obtained. Finally, the gels were dried at 120 °C for 10 h and heated at 1500 °C for 5 h to obtain the samples.

The phase of samples was checked with powder X-ray diffraction (XRD, Rigaku D/max2000, Dandong, China) with Cu Kα radiation (λ = 0.154178 nm, the scanning range of 20°-70°, voltage of 40 KV, and the current of 30 mA). The photoluminescence spectra were recorded on fluorescence spectrophotometer (F-4600, Hitachi, Japan) and a xenon lamp was used as the excitation source (voltage of 500 V and the scanning speed of 1200 nm/min). The powder morphology was observed with scanning electron microscope (SEM, JEOL-5600 LV, Japan). All the tests were completed at room temperature.

3. Results and discussion

Fig. 1 shows the XRD patterns of the samples obtained at different temperatures. When the calcination temperature is low, the diffraction intensity of the peaks is weak. The sample prepared at 1100 °C is mainly composed of $Ca_5(PO4)_2(SiO_4)$, $CaSiO_4$, and $Ca_3(PO4)_2$. With the rise of the synthesis temperature, the sample diffraction patterns are enhanced gradually and the crystallinity of the sample is continuously improved. According to the comparison results with a standard diffraction card, the diffraction peaks of the samples calcined at 1500 °C for 5 h can be well indexed to the phases of $Ca_7Si_2P_2O_{16}$ (JCPDS 11-0676). Therefore, the positions of XRD peaks show no obvious difference. $Ca_7Si_2P_2O_{16}$ has a hexagonal crystal structure with a space group $P6_1$ and its lattice constants are a=21.8Å, c=21.57Å, V=8877.56Å^3, and Z=24. The results indicate that this method can be used to synthesize single-phase samples of $Ca_7Si_2P_2O_{16}$:xEu^{3+}.

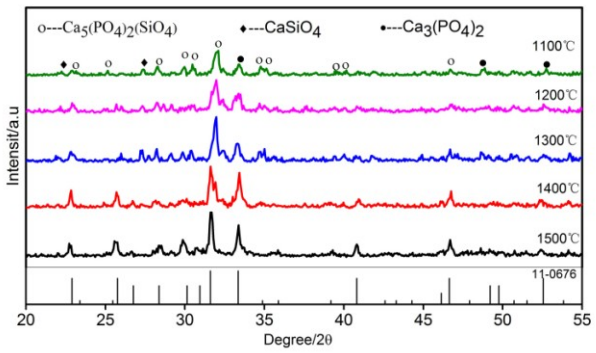

Fig. 1. XRD patterns of the samples calcined at different temperatures and standard card PDF2 No. 11-0676

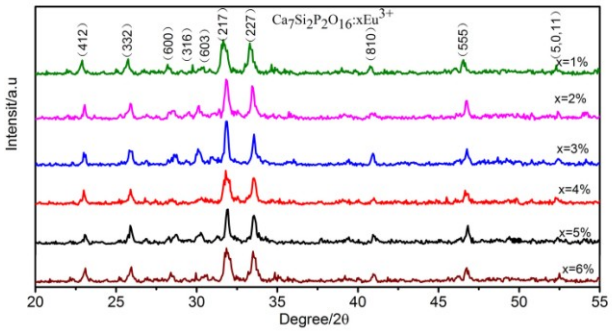

Fig. 2. XRD patterns of $Ca_7Si_2P_2O_{16}$:xEu^{3+} (x=1%-6%)

The influences of Eu^{3+} doping on XRD patterns of $Ca_7Si_2P_2O_{16}$:xEu^{3+} (x=1%-6%) are shown in Fig. 2. The doped Eu^{3+} did not generate any impurity or induce significant change in the $Ca_7Si_2P_2O_{16}$ lattice knot structure. With the increase in Eu^{3+} doping concentration, the diffraction intensity of (217) and (227) decreased gradually. The result indicated that Eu^{3+} had been successfully integrated into the host lattice. Eu^{3+} and Ca^{2+} have the similar radius. Therefore, Eu^{3+} is synthesized into the host lattice to substitute Ca^{2+} position in the sample and the distortion of $Ca_7Si_2P_2O_{16}$ matrix crystal lattice happens. Therefore, a small amount of Eu^{3+} has the less effect on the crystal structure when it enters the crystal lattice.

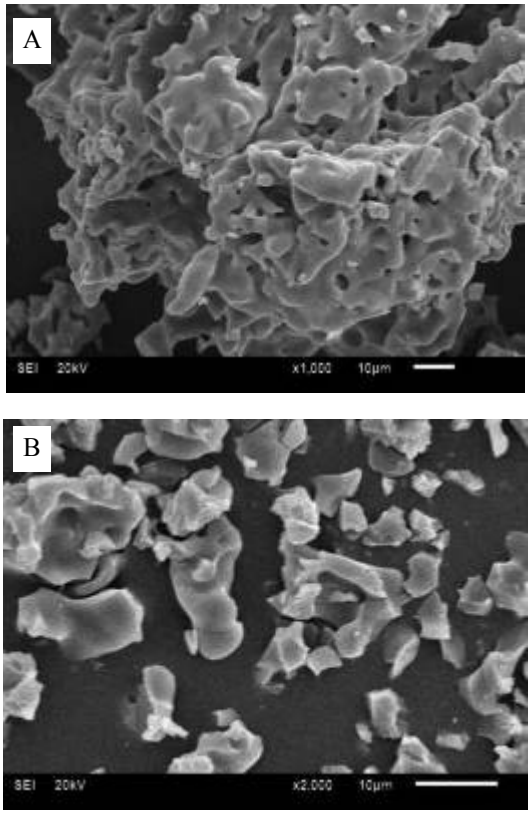

Fig. 3. SEM images of $Ca_7Si_2P_2O_{16}$:xEu^{3+} (x=5%)

Fig. 3 shows the SEM images of $Ca_7Si_2P_2O_{16}:xEu^{3+}$ (x=5%) samples of different regions. In the nearly block-shaped sample shown in Fig. 3(A), a little amount of reuniting on the edge of the sample was observed. Fig. 3(B) shows that the phosphors are relatively loose after calcination at 1500 °C and powder samples with the small size can be directly obtained without crushing and screening. The average particle size is about 5-10 μm. The particle size is appropriate and the brightness is high. The powder is suitable for the packaging of LED after full grinding.

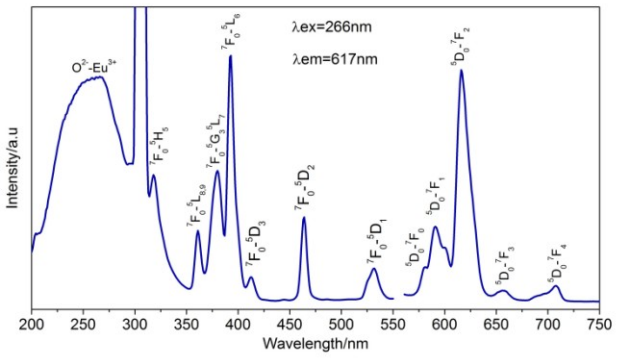

Fig. 4. Excitation and emission spectra of $Ca_7Si_2P_2O_{16}:xEu^{3+}$ (x=3%)

Fig. 4 presents the excitation and emission spectra of $Ca_7Si_2P_2O_{16}:xEu^{3+}$(x=3%) phosphors at room temperature. The excitation spectrum is monitored at the 617 nm and the result indicates that the excitation spectrum of Eu^{3+} can be divided into two parts. Firstly, a broadband excitation band between 210 and 310 nm with the peak at about 266 nm can be attributed to $O^{2-}\rightarrow Eu^{3+}$ charge transfer (Charge transfer band, CTB), generated by O^{2-} electron transition from a filled shell 2p orbital to $4f^6$ orbital of Eu^{3+} ions [24]. Secondly, the peaks between 310 nm and 600 nm can be attributed to the transition of Eu^{3+} f-f and the strongest excitation peak at 393 nm corresponds to the characteristic absorption peak of $^7F_0\rightarrow{}^5L_6$ transitions of Eu^{3+}. Meanwhile, other weak excitation peaks at 318 nm, 361 nm, 380 nm, 413 nm, 464 nm, and 532 nm, respectively correspond to the following electronic transitions: Eu^{3+} $^7F_0\rightarrow{}^5H_5$, $^7F_0\rightarrow{}^5L_{8,9}$, $^7F_0\rightarrow{}^5G_3{}^5L_7$, $^7F_0\rightarrow{}^5D_3$, $^7F_0\rightarrow{}^5D_2$, and $^7F_0\rightarrow{}^5D_1$. The ground state of Eu^{3+} is $^7F_0$ and the excited states include $^5D_0$ and $^5D_1$. In the transitions from $^5D_1$ and $^5D_0$ to ^7F_J (J=0-5), lights of various wavelengths are emitted. It can be clearly seen that the f-f transition of trivalent lanthanides is seldom affected by ligand ions in the crystals [10].

The emission spectra of the samples were excited at 266 nm. In the emission spectra, major fluorescent emission peaks at 581 nm, 592 nm, 617 nm, 656 nm, and 707 nm correspond to the following Eu^{3+} transition: $^5D_0\rightarrow{}^7F_0$, $^5D_0\rightarrow{}^7F_1$, $^5D_0\rightarrow{}^7F_2$, $^5D_0\rightarrow{}^7F_3$, and $^5D_0\rightarrow{}^7F_4$, respectively. The emission intensity of the transition $^5D_0\rightarrow{}^7F_2$ is stronger than that of the transitions $^5D_0\rightarrow{}^7F_1$, while the luminous intensity of the transitions $^5D_0\rightarrow{}^7F_0$, $^5D_0\rightarrow{}^7F_3$, and $^5D_0\rightarrow{}^7F_4$ is relatively weak. The emission spectrum is a line and the emission color with Eu^{3+} is irrelevant to the location of the lattice. According to the Judd-Ofelt theory, if the inversion symmetry central location is occupied by Eu^{3+}, the emission in the reddish orange zone will occur due to the magnetic transition in $^5D_0\sim{}^7F_1$ [25]; if Eu^{3+} occupies an non-inversion symmetry site, since $4f^6$ configuration is mixed with the opposite symmetric 5d configuration, due to crystal field inhomogeneity, the symmetrical crystals become wide. Therefore, the f-f transition is not available and the emission in the red zone occurs due to the transition $^5D_0\sim{}^7F_2$. The luminescence intensity of $Ca_7Si_2P_2O_{16}$ in a red emission ($^5D_0\sim{}^7F_2$) is stronger than that in reddish orange emission ($^5D_0\sim{}^7F_1$), indicating that Eu^{3+} occupies the non-inverse symmetric sites in $Ca_7Si_2P_2O_{16}$ crystals.

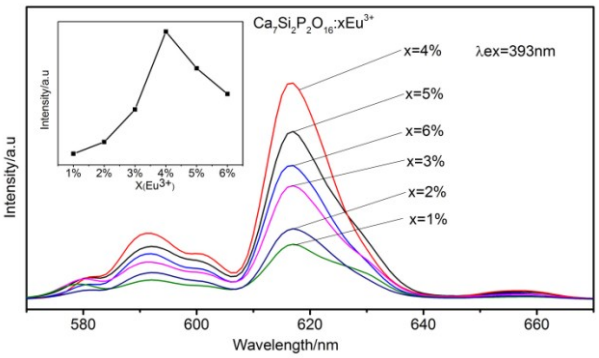

Fig. 5. Emission spectra of $Ca_7Si_2P_2O_{16}:xEu^{3+}$ samples with different Eu^{3+}-doping concentrations

To study the effects of Eu^{3+}-doping concentration on the luminescence intensity, a series of $Ca_7Si_2P_2O_{16}:xEu^{3+}$ samples with different Eu^{3+} doping concentrations were prepared under the same conditions. The emission spectra (λex=393nm) and emission intensities of $Ca_7Si_2P_2O_{16}xEu^{3+}$ phosphors are shown in Fig. 5. With the increase in the Eu^{3+}-doping concentration, the emission density of Eu^{3+} shows no significant change, but the luminous intensity shows the significant change. As shown in Fig. 5, with the increase in the Eu^{3+}-doping concentration, the luminescence intensity is enhanced and reaches its maximum at x=4%. When the Eu^{3+}-doping concentration is further increased (x>4%), the luminescence intensity decreases. When Eu^{3+} concentration is low, the incorporated Eu^{3+} amount is less than the number of active ions and is not enough to form a luminescent center, thus leading to the lower emission intensity. With the increase in the Eu^{3+} -doping concentration, the number of luminescent centers is also increased and the luminous intensity starts to increase. When x=4%, the luminous intensity is the strongest.

When the Eu^{3+}-doping concentration is increased above 4%, the emission intensity begins to drop. The concentration of 4% is the quenching concentration. The phenomenon can be interpreted as follows. Firstly, the cross relaxation among active Eu^{3+} causes energy loss in the excitation emission level. With the decrease in the distance among Eu^{3+}, the energy transfer among Eu^{3+} ions becomes easier, thus enhancing the interaction and the energy transfer and leading to the decrease in the emission intensity.

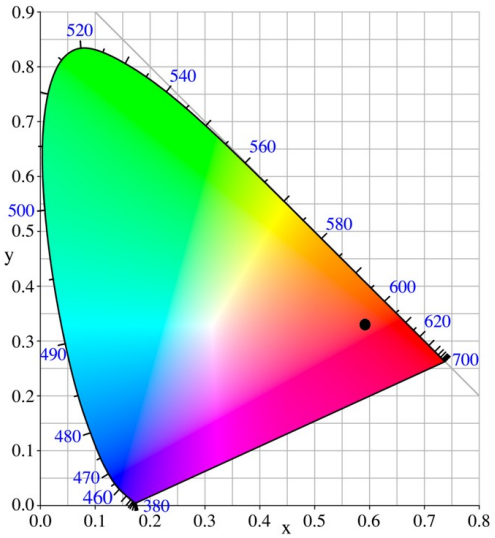

Fig. 6. CIE color coordinates of $Ca_7Si_2P_2O_{16}$:4%Eu^{3+}

Fig. 6 shows the color coordinate diagram of $Ca_7Si_2P_2O_{16}$:4%Eu^{3+}. The CIE chromaticity coordinates of the red LED were calculated to be (0.5921, 0.3292). The calculated coordinates are located in the red zone.

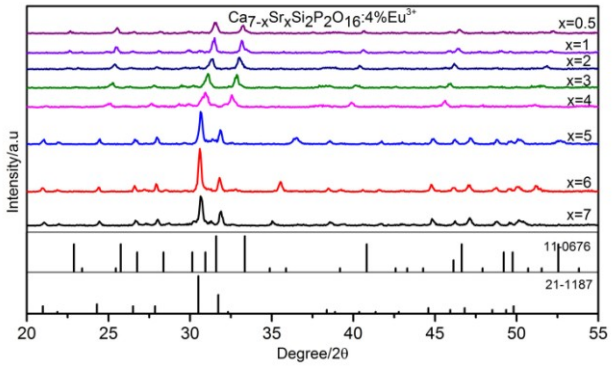

Fig. 7. XRD patterns of $Ca_{7-x}Sr_xSi_2P_2O_{16}$:4%$Eu^{3+}$ (x=0.5-7%) and standard card PDF2 No. 11-0676 and No. 21-1187

In order to examine the effect of Sr^{2+} ion replacement on the luminescence intensity, a series of $Ca_{7-x}Sr_xSi_2P_2O_{16}$:4%$Eu^{3+}$ samples with different Sr^{2+} doping concentrations were prepared. The influences of Sr^{2+} content on $Ca_{7-x}Sr_xSi_2P_2O_{16}$:4%$Eu^{3+}$ XRD patterns are shown in Fig. 7. When the X is less than 4, the shapes of the diffraction peaks show no obvious change, but the positions of the diffraction peaks is gradually shifted to the left. When the x is greater than 4, the position of the diffraction peak is large. The peaks can be well matched with the standard card (21-1187 JCPDS). It is conducive to the formation of $Sr_5(PO_4)_2(SiO_4)$. According to the Prague equation: $2d\sin\theta=n\lambda$, the interplanar distance increases because the radius of Sr^{2+} is slightly larger than that of Ca^{2+}, thus resulting in the decreased θ. The diffraction peak shifts to the left. When the x is more than 5, the diffraction peak is significantly shifted to the left and can be well indexed to the phases of $Sr_5(PO_4)_2(SiO_4)$ (JCPDS 21-1187), indicating that the synthesis conditions are favorable to the formation of the compounds of Sr^{2+}.

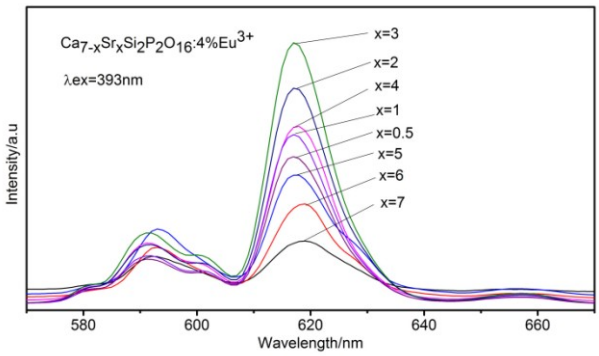

Fig. 8. Emission spectra of $Ca_{7-x}Sr_xSi_2P_2O_{16}$:4%$Eu^{3+}$

Fig. 8 shows the emission spectra of $Ca_{7-x}Sr_xSi_2P_2O_{16}$:4%$Eu^{3+}$ phosphors. With the increase in the Sr^{2+} ion replacement concentration, the luminescence intensity is enhanced gradually and reaches its maximum value at the x=3 and the intensity is about two times more than that of the samples before replacement. The radius of Sr^{2+} is larger than that of Ca^{2+}, thus leading to the greater lattice distortion with the increase in the Sr^{2+} ion concentration. At the same time, the luminescent centers are also increased and the luminous intensity starts to rise.

4. Conclusions

$Ca_{7-x}Sr_xSi_2P_2O_{16}$:$Eu^{3+}$ red phosphor was successfully synthesized through the sol-gel method and its photoluminescence properties were also studied. The single insulation $Ca_7Si_2P_2O_{16}$ phase was prepared after calcination at 1500 °C for 5 h. The final products displayed two emission peaks at 593 nm and 618 nm, indicating that Eu^{3+} ions occupied several different sites in the crystals. According to the monitoring results of these two emission peaks, we found several peaks at 252 nm, 361 nm, 380 nm, and 393 nm and several broadband excitation spectra. The main excitation peak at 393 nm was consistent with the UVLED wavelength. Moreover,

with the increase in the Eu^{3+} ion concentration, the emission intensity gradually increased; when the Eu^{3+} ion concentration was increased above 4%, the spectral intensity decreased. After the addition of Sr^{2+}, the intensity of the emission spectrum had been improved significantly. As a typical phosphor, $Ca_7Si_2P_2O_{16}:xEu^{3+}$ is a good red luminescent material in the silicon phosphate material field.

Acknowledgment

This work was jointly supported by the State-owned Enterprises and University Cooperation Key Projects of Sichuan Province (Grant No. 80303-SZL021) and the Science and Technology Department Project of Sichuan Province (2014GZ0090-Z3).

References

[1] S. Chen, X. Liu, M. Gu, C. Ni, B. Liu, S. Huang, J. Lumin. **140**, 1 (2013).
[2] H. B. Premkumar, H. Nagabhushana, S. C. Sharma, S. C. Prashantha, H. P. Nagaswarupa, B. M. Nagabhushana, R.P.S. Chakradhar, J. Alloy. Compd. **601**, 75 (2014).
[3] Z. Chen, J. H. Zhang, S. Chen, M. Y. Lin, C. Q. He, G. D. Xu, M. M. Wang, X. F. Yu, J. Q. Zou, K. Guo, J. Alloy. Compd. **632**, 756 (2015).
[4] V. Kumar, S. Singh, S. Chawla, Superlattice. Microst **79**, 86 (2015).
[5] J. Zhao, Y. Wu, Y. Liang, M. Liu, F. Yang, Z. Xia, Opt. Mater. **35**, 1675 (2013).
[6] J. Huang, B. Hou, H. Ling, J. Liu, X. Yu, Inorg. Chem. **53**, 9541 (2014).
[7] F. Chen, X. Liu, Opt. Mater. **35**, 2716 (2013)
[8] H. Lai, A. Bao, Y. Yang, Y. Tao, H. Yang, J. Nanopart. Res. **10**, 1335 (2008).
[9] S. Demirci, S. Gültekin, S. A. Akalin, Ö. Öter, K. Ertekin, E. Çelik, Mat. Sci. Semicon. Proc. **611**, 31 (2015).
[10] K. Y. Hwan, L. S. Hyun, Y. J. Su, J. Nanosci. Nanotechno. **13**, 3230 (2013)
[11] J. Wang, L. Qin, Y. Huang, D. Wei, H. Seo, Applied. Physics. A. **1215**, 115 (2014).
[12] D. Wei, Y. Huang, S. I. Kim, Y. M. Yu, H. J. Seo, Mater. Lett. **122**, 99 (2013).
[13] Y. Zhai, S. Feng, Z. Zhang, L. Shi, X. He, Rare. Met. Mater. **1825**, 39 (2010).
[14] H. Liu, D. He, F. Shen, J. Rare. Earth. **121**, 24 (2006).
[15] T. Kim, T. Kim, J. Kim, S. Kim, S. Im, J. Phys. Chem. **12428**, 118 (2014).
[16] S. Hur, H. J. Song, H. Roh, D. Kim, K. S. Hong, Mater. Chem. Phys. **350**, 139 (2013).
[17] H. Yu, D. Deng, Y. Li, S. Xu, Y. Li, C. Yu, Y. Ding, H. Lu, H. Yin, Q. Nie, Opt. Commun. **103**, 289 (2013).
[18] H. Roh, S. Hur, H. J. Song, I. J. Park, D. K. Yim, D. Kim, K. S. Hong, Mater. Lett. **37**, 70 (2012).
[19] X. Wang, J. Gan, Y. Huang, H. J. Seo, Ceram. Int. **701**, 38 (2012).
[20] S. Xin, Y. Wang, G. Zhu, F. Zhang, Y. Gong, Y. Wen, B. Liu, Mater. Res. Bull. **1627**, 48 (2013).
[21] J. Gan, Y. Huang, L. Shi, X. Qiao, H. J. Seo, Mater. Lett. **2160**, 63 (2009).
[22] D. Wei, Y. Huang, H. J. Seo, Mater. Res. Bull. **3614**, 48 (2013).
[23] Y. Shi, G. Zhu, M. Mikami, Y. Shimomura, Y. Wang, Opt. Mater. Express. **280**, 4 (2014).
[24] F. Shang-yi, G.. Mu, L. Xiao-lin, N. Chen, L. Bo, H. Shi-ming, Spectrosc. Spect. Anal **30**, 2317 (2010).
[25] P. Woo-Jung, J. Mong-Kwon, M. Ji-Wook, M. Takaki, I. Seong-Jae,Y. Dae-Ho, J. Nanosci, Nanotechno. **9**, 4371 (2009).

*Corresponding author: lijunfeng@cdut.edu.cn